ELSEVIER

J. Non-Newtonian Fluid Mech. 108 (2002) 99–122

Journal of Non-Newtonian Fluid Mechanics

www.elsevier.com/locate/jnnfm

Adaptive configuration fields: a new multiscale simulation technique for reptation-based models with a stochastic strain measure and local variations of life span distribution☆

Piyush G. Gigras, Bamin Khomami*

Department of Chemical Engineering, The Materials Research Laboratory, Washington University, St. Louis, MO 63130-4899, USA

Abstract

In this work a new multiscale simulation technique, i.e. Adaptive configuration fields method (ACFM), has been proposed for complex flow simulation of state-of-the-art reptation-based models for entangled polymeric systems. Specifically, this technique combines the essential aspects of the previously introduced Brownian configuration fields and the deformation fields methods [J. Non-Newtonian Fluid Mech. 70 (1997) 79; J. Non-Newtonian Fluid Mech. 89 (2000) 209] to allow simulation of advanced reptation models with a stochastic strain measure and local variations of life span distribution. In order to examine the fidelity and robustness of our new simulation technique, we have performed simulations in a number of different fixed kinematics flows using the single segment reptation model of Öttinger [J. Rheol. 44 (2000) 1293], which possesses the essential features required for quantitatively describing the non-linear rheology of polymer melts, but cannot be implemented in a complex flow using the available state-of-the-art Eulerian multiscale simulation techniques, namely, the Brownian configuration fields or the deformation fields. In turn, the simulation results in unidirectional flows are compared with pure Brownian dynamics simulations and it is shown that the results are in excellent agreement, thus verifying the accuracy of the adaptive configuration fields method.

Keywords: Reptation; Configuration fields; Deformation fields; Entangled polymeric systems; Simulation algorithm

1. Introduction

Theories based on the concept of reptation proposed by de Gennes [1] have emerged as a primary tool for describing the rheology for entangled polymers. Doi and Edwards [2–5] were the first investigators

☆ Paper presented at the XIIth International workshop on numerical methods in viscoelastic flows, Monetery Bay, CA, July 15–17, 2002. Dedicated to the memory of Piyush G. Gigras.

* Corresponding author. Fax: +1-314-935-7211.

E-mail address: bam@poly1.che.wustl.edu (B. Khomami).

0377-0257/02/$ – see front matter
PII: S0377-0257(02)00126-X

to use the concept of reptation to develop a theory for rheology of entangled polymers. The original reptation-based model by Doi and Edwards [2–5] has deficiencies such as excessive shear thinning in fast shearing flows, however, most of the deficiencies of this model can be traced back to a number of assumptions such as instantaneous and complete chain retraction, "independent alignment" of different parts of the chain, single relaxation mechanism and no chain stretch that were used to arrive at a closed form constitutive equation [6,7].

Recent advances in the reptation theories have largely resolved long-standing deficiencies in the Doi–Edwards (DE) model's ability to describe the non-linear rheology of entangled linear polymers. Specifically, "double reptation (DR)" [8,9] and "convective constraint release (CCR)" [10,11] have been shown to play an important role in the relaxation mechanism. Moreover, chain stretch has been shown [12] to greatly influence the non-linear rheology of entangled polymeric systems. Various theories that include these effects, while avoiding the "independent alignment" assumption have been proposed. These theories can be broadly classified in two categories distinguished by their segment connectivity concepts. Under the first category, come those models which have been developed within the scope of a single segment description. The recently introduced models of Marucci–Greco–Ianniruberto (MGI) [13], Öttinger [7,14] and the "simplified" model of Mead–Larson–Doi (MLD) [15] fall in this category. Under the second category are those models which rely heavily on the segment connectivity concept. The model of Hua–Schieber–Venerus [6,16,17], and the "contour variable" MLD model [15] which give a full chain description in conjunction with constraint release mechanisms, come under this category. Since in these models the motion of each segment in the chain is considered, they can be used to understand how various mechanisms, e.g. convective constraint release, chain stretching, etc. influence the flow properties of entangled polymeric systems.

Although, the full chain models perform exceptionally well in describing the subtle details of shear rheology of entangled polymers, they are highly computationally intensive. Hence, flow simulations of entangled polymeric systems to date have been limited to single segment theories. In particular, van den Brule and coworkers [18,19] have used the Brownian configuration fields (BCF) [20] and the deformation fields (DF) methods [21] for simulating flow of reptation-based models in complex geometries. Specifically, they have considered flow of the DE model as well as more advanced reptation models such as the "simplified" MLD model. Similarly, Wapperom and Keunings [22] have used the DF method to simulate the MGI model. However, these techniques cannot be used to simulate flow of reptation-based models with a stochastic strain measure and local variations of life span distribution such as the Öttinger model. Since the Öttinger model makes very similar predictions as the full chain model of Schieber and coworkers [6,16,17] at a dramatic computational savings, a methodology for simulating this single segment reptation model is highly desirable. Considering the fact that the traditional techniques (i.e. BCF and DF) cannot be used, one must either resort to Lagrangian methods such as CONNFFESSIT [23], variance reduced CONNFFESSIT [24] or Lagrangian particle methods [25–27] or devise a new Eulerian-based technique that overcomes the limitations of the BCF and DF techniques. Since Eulerian-based methods are ideally suited for implementation within a finite element context and circumvent the use of CPU intensive particle tracking methods, we have focused our attention on developing a new Eulerian simulation method that allows for a stochastic strain measure and local variations of life span distribution.

The paper is organized as follows: Section 2 gives a brief description of the Öttinger's single segment reptation model. The shortcomings of the BCF and DF methods in simulating advanced reptation models with a stochastic strain measure and local variations of life span distribution are discussed in Section 3. In Section 4 we describe our new simulation algorithm, namely, the "adaptive configuration fields method".

In order to demonstrate the accuracy of our simulation technique, computations in several unidirectional flows are performed in Section 5 and the results are compared with the Brownian dynamics simulation results. Finally, conclusions are presented in Section 6.

2. Öttinger's single segment reptation model

As mentioned earlier, Öttinger and coworkers have recently developed a single segment reptation model that describes the non-linear rheology of entangled polymers. In this work, we have chosen the most recent version of the model [7] that assumes uniform monomer density and isotropic tube cross-section. For this model the time evolution equation of the chain stretch variable is given by

$$\frac{D\lambda}{Dt} = \dot{\lambda}_{\text{conv}} + \dot{\lambda}_{\text{dissip}} \tag{2.1}$$

where,

$$\dot{\lambda}_{\text{conv}} = \lambda \boldsymbol{\kappa} : \boldsymbol{\tau} \quad \dot{\lambda}_{\text{dissip}} = \frac{1}{\tau_{\text{s}}} \frac{c(\lambda)}{3Z} (\lambda - 1), \quad c(\lambda) = \frac{3Z\lambda_{\text{max}}^2(\lambda + 1)}{\lambda(\lambda_{\text{max}}^2 - \lambda^2)} \tag{2.2}$$

and, the Fokker Planck Equation, describing the distribution of the polymer configurations, supplemented with the boundary conditions of random orientation at the chain ends, is given by

$$\begin{aligned} \frac{Df}{Dt} = &-\frac{\partial}{\partial \boldsymbol{u}} \cdot \left[\left(\boldsymbol{\delta} - \frac{\boldsymbol{u}\boldsymbol{u}}{|\boldsymbol{u}|^2} \right) \cdot \boldsymbol{\kappa} \cdot \boldsymbol{u} f \right] + \frac{\partial}{\partial \boldsymbol{u}} \cdot \mathcal{D} \left(\boldsymbol{\delta} - \frac{\boldsymbol{u}\boldsymbol{u}}{|\boldsymbol{u}|^2} \right) \cdot \frac{\partial}{\partial \boldsymbol{u}} f \\ &+ \frac{1}{\pi^2 \tau_{\text{d}}} \frac{\partial^2 f}{\partial s^2} - \frac{\partial}{\partial s} (\dot{s}_{\text{tot}} f) - \frac{\dot{\lambda}_{\text{dissip}}}{\lambda} f \end{aligned} \tag{2.3}$$

$$f = \frac{1}{4\pi} \delta(|\boldsymbol{u}| - 1), \quad s = 0, 1 \tag{2.4}$$

where,

$$\dot{s}_{\text{tot}} = -\frac{1}{\lambda} \left[s - \frac{1}{2} \right] \dot{\lambda}_{\text{dissip}} \tag{2.5}$$

$$\mathcal{D} = \frac{1}{6} \left[\delta_1 \frac{1}{\tau_{\text{d}}} - \delta_2 \frac{\dot{\lambda}_{\text{dissip}}}{\lambda} H \left(-\frac{\dot{\lambda}_{\text{dissip}}}{\lambda} \right) \right] \tag{2.6}$$

In the above set of equations, λ is the stretch parameter that denotes the ratio of chain contour length to the equilibrium contour length, $\dot{\lambda}_{\text{conv}}$ and $\dot{\lambda}_{\text{dissip}}$ are the convective and dissipative contributions to the evolution of the stretch parameter respectively, f is the configuration distribution function, $\boldsymbol{u}$ the normalized unit vector describing the orientation of a tube segment with $s \in [0,1]$ being the position label of the segment, $\boldsymbol{\kappa}$ the transpose of the velocity gradient tensor, $\boldsymbol{\tau} = \langle \boldsymbol{u}\boldsymbol{u} \rangle$ the second moment orientation tensor, Z the number of entanglements per chain, τ_{s} the characteristic stretching time, $c(\lambda)$ the spring coefficient, which models the elastic nature of the polymer molecules, λ_{max} the maximum possible stretching ratio of the chain contour length, $\dot{s}_{\text{tot}}$ the drift velocity for s, $\mathcal{D}$ the orientational diffusion coefficient due to the constraint release mechanisms, δ_1 and δ_2 are the parameters representing double reptation and convective constraint release mechanisms, respectively, τ_{d} is the reptation time and H is the heaviside step function.

The polymeric stress, $\boldsymbol{\tau}(t)$, in this model, is evaluated using the following Kramers type expression, which includes the original Doi–Edwards part and the added contribution due to the fact that the chain can be stretched:

$$\boldsymbol{\tau}(t) = 3Zn_{\mathrm{p}}k_{\mathrm{B}}T\left[1 + \frac{c(\lambda(t))\lambda(t)(\lambda(t)-1)}{3Z}\right]\int_0^1\int_{\boldsymbol{u}}\boldsymbol{u}\boldsymbol{u}\,f(\boldsymbol{u},s)\,\mathrm{d}\boldsymbol{u}\,\mathrm{d}s \tag{2.7}$$

where, n_{p} is the number density of polymers, k_{B} is the Boltzmann's constant and T is the temperature. Eq. (2.1) through Eq. (2.7) can be used to determine the polymeric stress. The corresponding equivalent (without considering the creation/destruction term in the Fokker Planck Equation) stochastic differential equations (SDEs) are given by

$$\mathrm{d}\boldsymbol{u}_t = \left[\left(\boldsymbol{\delta} - \frac{\boldsymbol{u}_t\boldsymbol{u}_t}{|\boldsymbol{u}_t|^2}\right)\cdot\boldsymbol{\kappa}\cdot\boldsymbol{u}_t - 2\mathcal{D}\boldsymbol{u}_t\right]\mathrm{d}t + \sqrt{2\mathcal{D}}\left(\boldsymbol{\delta} - \frac{\boldsymbol{u}_t\boldsymbol{u}_t}{|\boldsymbol{u}_t|^2}\right)\cdot\mathrm{d}\boldsymbol{W}_t \tag{2.8}$$

$$\mathrm{d}s_t = \dot{s}_{\mathrm{tot}}\,\mathrm{d}t + \frac{1}{\pi}\sqrt{\frac{2}{\tau_{\mathrm{d}}}}\mathrm{d}W_t' \tag{2.9}$$

where $\boldsymbol{u}_t$ and s_t are the stochastic processes equivalent to $\boldsymbol{u}$ and s, respectively and $\boldsymbol{W}_t$ and $\boldsymbol{W}_t'$ are independent Wiener processes. The stress, $\boldsymbol{\tau}(t)$, can equivalently be obtained by performing Brownian dynamics simulations with the above SDEs for $\boldsymbol{u}_t$ and s_t, in combination with Eq. (2.1),

$$\frac{\boldsymbol{\tau}(t)}{3Zn_{\mathrm{p}}k_{\mathrm{B}}T\left[1+\frac{c(\lambda)\lambda(\lambda-1)}{3Z}\right]} = \int_0^1\int_{\boldsymbol{u}}\boldsymbol{u}\boldsymbol{u}\,f(\boldsymbol{u},s)\,\mathrm{d}\boldsymbol{u}\,\mathrm{d}s = \langle\boldsymbol{u}_t\boldsymbol{u}_t\rangle \tag{2.10}$$

For details we refer the reader to the original paper by Fang et al. [7].

3. Limitations of the BCF and DF techniques for simulation of reptation models with a stochastic strain measure and local variations of life span distribution

3.1. The Brownian configuration fields method

In the BCF method, the polymer configuration distribution is represented by a collection of configuration fields, each of which evolves according to the material counter part of the SDE governing individual members of the ensemble. The stress at any point in the flow domain is obtained by the second moment of the fields evaluated at that point. Van Heel et al. [18] have used this technique to perform complex flow simulations of the DE model. The essential idea is to introduce N vector fields, $\boldsymbol{u}_k(\boldsymbol{x}, t)$ ($k = 1, 2, 3, \ldots, N$), to describe the tube segmental orientation, where '$\boldsymbol{x}$' specifies the spatial position within the flow domain, along with individual random walkers, S_k ($k = 1, 2, 3, \ldots, N$) associated with each vector field. The fields and random walkers evolve according to the SDE equivalent of the DE model

$$\mathrm{d}\boldsymbol{u}_t = \left[\left(\boldsymbol{\delta} - \frac{\boldsymbol{u}_t\boldsymbol{u}_t}{|\boldsymbol{u}_t|^2}\right)\cdot\boldsymbol{\kappa}\cdot\boldsymbol{u}_t\right]\mathrm{d}t \tag{3.1}$$

$$\mathrm{d}s_t = \frac{1}{\pi}\sqrt{\frac{2}{\tau_{\mathrm{d}}}}\mathrm{d}W_t \tag{3.2}$$

Note that, unlike the Öttinger's model, the evolution of the tube is purely deterministic. Also, the evolution of the primitive chain is purely stochastic and spatially uniform. The combination of these facts allow the use of concept of BCF for simulation of the original DE model. Specifically, the BCF representation of the SDE for the configuration fields is given by:

$$\frac{\partial}{\partial t}\boldsymbol{u}_k(\boldsymbol{x},t)+\boldsymbol{v}(\boldsymbol{x},t)\cdot\nabla\boldsymbol{u}_k(\boldsymbol{x},t) = \left(\boldsymbol{\delta}-\frac{\boldsymbol{u}_k(\boldsymbol{x},t)\boldsymbol{u}_k(\boldsymbol{x},t)}{|\boldsymbol{u}_k(\boldsymbol{x},t)|^2}\right)\cdot\boldsymbol{\kappa}(\boldsymbol{x},t)\cdot\boldsymbol{u}_k(\boldsymbol{x},t), \quad k=1,2,3,\ldots,N \tag{3.3}$$

where $\boldsymbol{v}$ is the velocity field. The simulation is started by assigning individual random unit vectors to each of the configuration fields along with individual random number $\in$ [0,1] to each of the random walkers S_k. This implies that initially each field is spatially uniform. As the simulation proceeds in time, the fields evolve according to Eq. (3.3) changing with the local velocity gradient. At the same time, the random walkers perform Brownian motion and get updated according to Eq. (3.2). Each time the random walker gets reflected (S_k reaches the boundary at 0 or 1), the entire field, to which the random walker had been assigned to, is replaced by a new spatially uniform field. The simplicity of this method lies in the fact that not only is the tube equation purely determinstic, which keeps the fields highly correlated during the course of a simulation and hence reduces the statistical error, but even the individual random walkers are easy to simulate since they are purely stochastic and not a function of position. In turn, stress at any point in the flow domain is evaluated by taking an average $\langle \boldsymbol{u}_k(\boldsymbol{x},t)\boldsymbol{u}_k(\boldsymbol{x},t)\rangle$ over all the fields.

In what follows, we will briefly describe why the BCF method is not suitable for performing simulations with the Öttinger model. First, this model has an additional variable associated with chain stretching, i.e. λ. However, the chain stretch variable λ only appears as a function of position in the SDE, hence one can define a stretch field variable, $\lambda(\boldsymbol{x},t)$, that is continuous over the entire domain of interest. The evolution equation for the stretch field is given by

$$\frac{\partial}{\partial t}\lambda(\boldsymbol{x},t)+\boldsymbol{v}(\boldsymbol{x},t)\cdot\nabla\lambda(\boldsymbol{x},t)=\lambda(\boldsymbol{x},t)\boldsymbol{\kappa}(\boldsymbol{x},t):\boldsymbol{\tau}(\boldsymbol{x},t)-\frac{1}{\tau_s}\frac{c(\lambda(\boldsymbol{x},t))}{3Z}(\lambda(\boldsymbol{x},t)-1) \tag{3.4}$$

$$\lambda(\boldsymbol{x},t=0)=1 \tag{3.5}$$

Clearly, the presence of the stretch variable does not limit the usefulness of the BCF method. However, if we now define configuration fields, $\boldsymbol{u}_k(\boldsymbol{x},t)$ ($k=1,2,3,\ldots,N$), for the tube segmental orientations along with individual random walkers, S_k ($k=1,2,3,\ldots,N$), the corresponding SDEs for the Öttinger model become

$$\begin{aligned}\frac{\partial}{\partial t}\boldsymbol{u}_k(\boldsymbol{x},t)+\boldsymbol{v}(\boldsymbol{x},t)\cdot\nabla\boldsymbol{u}_k(\boldsymbol{x},t) &= \left(\boldsymbol{\delta}-\frac{\boldsymbol{u}_k(\boldsymbol{x},t)\boldsymbol{u}_k(\boldsymbol{x},t)}{|\boldsymbol{u}_k(\boldsymbol{x},t)|^2}\right)\cdot\boldsymbol{\kappa}(\boldsymbol{x},t)\cdot\boldsymbol{u}_k(\boldsymbol{x},t)-2\mathcal{D}(\boldsymbol{x},t)\boldsymbol{u}_k(\boldsymbol{x},t)\\ &\quad+\sqrt{2\mathcal{D}(\boldsymbol{x},t)}\left(\boldsymbol{\delta}-\frac{\boldsymbol{u}_k(\boldsymbol{x},t)\boldsymbol{u}_k(\boldsymbol{x},t)}{|\boldsymbol{u}_k(\boldsymbol{x},t)|^2}\right)\cdot\frac{\mathrm{d}\boldsymbol{W}_t}{\mathrm{d}t}\end{aligned} \tag{3.6}$$

$$\frac{\partial}{\partial t}S_k(\boldsymbol{x},t)+\boldsymbol{v}(\boldsymbol{x},t)\cdot\nabla S_k(\boldsymbol{x},t)$$
$$=\frac{1}{\lambda(\boldsymbol{x},t)}\left[S_k(\boldsymbol{x},t)-\frac{1}{2}\right]\frac{1}{\tau_s}\frac{c(\lambda(\boldsymbol{x},t))}{3Z}(\lambda(\boldsymbol{x},t)-1)+\frac{1}{\pi}\sqrt{\frac{2}{\tau_d}\frac{\mathrm{d}W_t'}{\mathrm{d}t}} \tag{3.7}$$

A close examination of the above equations clearly shows the inadequacy of the BCF method for simulating the Öttinger model. Unlike the original DE model, the local velocity gradient now has an influence (through the stretch variable $\lambda(\boldsymbol{x}, t)$) on the evolution of the variable, S_k. This is a serious drawback, since reflections in S_k are dependent on both time and space. This would mean that it is not possible to replace the entire field upon the reflection of the S_k variable at a certain location, because it is highly unlikely that the tube completes its life span at the same time for all the locations in the flow domain. In other words, the fact that the tube survival probability is different at different locations in the flow domain is the reason why the BCF method cannot be used in simulating Öttinger's model. However, it should be noted that the evolution of the fields (Eq. (3.6)) can still be easily performed using the BCF method. In fact, in our new approach we will use Eq. (3.6) to simulate the evolution of the configuration fields associated with the tube segmental orientation.

3.2. The deformation fields method

In the DF method, the stress is obtained from an equation similar to the following time–strain separable integral constitutive equation, which represents the tracking of the deformation experienced by the molecules as a function of time and calculating the stress from it

$$\boldsymbol{\tau}(\boldsymbol{x},t)=\int_{-\infty}^{t}M(t-t')g[\boldsymbol{B}_{t'}(\boldsymbol{x},t)]\,\mathrm{d}t' \tag{3.8}$$

In the above equation, $M(t-t')$ is the memory function and $g[\boldsymbol{B}_{t'}(\boldsymbol{x},t)]$ is a tensorial function which provides the strain measure. Application of the deformation fields method in simulating reptation models has been discussed at length by van Heel et al. [18] and Peters et al. [19]. The essential idea in the DF method is to introduce and propagate "deformation fields", $\boldsymbol{B}_{t'}(\boldsymbol{x},t)$, each labeled by their time of creation, t', and then weigh the contribution of various individual deformation fields with the help of the memory function, $M(t-t')$, so as to finally calculate the total stress, $\tau(\boldsymbol{x},t)$, utilizing Eq. (3.8). The fields, as in the BCF method, are again thought of as a continuous variable in the Eulerian sense, and therefore evolve according to the following equation:

$$\frac{\partial}{\partial t}\boldsymbol{B}_{t'}(\boldsymbol{x},t)+\boldsymbol{v}(\boldsymbol{x},t)\cdot\nabla\boldsymbol{B}_{t'}(\boldsymbol{x},t)=\boldsymbol{\kappa}(\boldsymbol{x},t)\cdot\boldsymbol{B}_{t'}(\boldsymbol{x},t)+\boldsymbol{B}_{t'}(\boldsymbol{x},t)\cdot\boldsymbol{\kappa}^{\mathrm{T}}(\boldsymbol{x},t) \tag{3.9}$$

where, t' denotes the time in the past from which $\boldsymbol{B}_{t'}(\boldsymbol{x},t)$ contains the deformation history of flow. The DF method is more efficient than the BCF method because it avoids the requirement of recording individual tube deformations, which is an integral part of the BCF method. $\boldsymbol{B}_{t'}(\boldsymbol{x},t)$ contains all the information regarding the deformation of those tubes which were born at this time, t', and therefore the orientations of such tubes at the present time, t, can be easily found from their initial orientation and their deformation thereafter, $\boldsymbol{B}_{t'}(\boldsymbol{x},t)$.

The DE model can be easily written in the form of Eq. (3.8)

$$\boldsymbol{\tau}(\boldsymbol{x},t) = 3Zn_{\mathrm{p}}k_{\mathrm{B}}T\int_{-\infty}^{t}\left[\int_{0}^{1}\left(\frac{\partial K(\boldsymbol{x},t,t',s)}{\partial t'}\right)\mathrm{d}s\right]\langle \boldsymbol{u}(\boldsymbol{x},t)\boldsymbol{u}(\boldsymbol{x},t)\rangle_{t'}\,\mathrm{d}t' \tag{3.10}$$

where, $K(\boldsymbol{x},t,t',s)$ is the probability that a tube segment which was created at or before time t' still exists at the present time t. The term inside the angular brackets represents the orientation of those tubes, which were born at or before time t', at the present time. This is the orientation tensor, that provides the strain measure. Utilizing the independence between the process '$\boldsymbol{u}$' and 's' one can determine both the memory function and the strain measure for the DE model by integrating the diffusion equation for the probability distribution function of the DE model and subsequently solving the resulting differential equation for the $K(\boldsymbol{x},t,t',s)$ and '$\boldsymbol{u}$' [4,28]. Following this procedure, the memory function and the strain measure for the DE model (i.e. apart from an overall multiplicative factor of $3Zn_{\mathrm{p}}k_{\mathrm{B}}T$) are given by

$$M(t-t') = \frac{8}{\pi^2\tau_{\mathrm{d}}}\sum_{n=1}^{\infty}\mathrm{e}^{-(2n-1)^2(t-t')/\tau_{\mathrm{d}}} \tag{3.11}$$

$$g[\boldsymbol{B}_{t'}(\boldsymbol{x},t)] = \left\langle \frac{\boldsymbol{B}_{t'}^{1/2}(\boldsymbol{x},t)\cdot\boldsymbol{u}(t')\boldsymbol{B}_{t'}^{1/2}(\boldsymbol{x},t)\cdot\boldsymbol{u}(t')}{|\boldsymbol{B}_{t'}^{1/2}(\boldsymbol{x},t)\cdot\boldsymbol{u}(t')|^2}\right\rangle_{t'} \tag{3.12}$$

where, $\boldsymbol{u}(t')$ is the initial tube orientation of an ensemble member. Given the initial tube orientation, $\boldsymbol{u}(t')$, and the deformation it experiences thereafter, $\boldsymbol{B}_{t'}^{1/2}(\boldsymbol{x},t)$, the strain measure, $g[\boldsymbol{B}_{t'}(\boldsymbol{x},t)]$, can be easily evaluated from the above equation by taking an ensemble average. The polymeric stress at any time t can thus be calculated from Eq. (3.10) using Eqs. (3.11) and (3.12). Hence, the DE model can be easily simulated using the DF method. Following the same strategy, in what follows we will attempt to determine the memory function and the strain measure for the Öttinger's model. If we succeed, we shall be able to utilize the DF method for complex flow simulations of the Öttinger's model. For this model, one can write down the stress equation in a similar fashion as Eq. (3.10)

$$\frac{\boldsymbol{\tau}(\boldsymbol{x},t)}{3Zn_{\mathrm{p}}k_{\mathrm{B}}T} = \left[1+\frac{c(\lambda)\lambda(\lambda-1)}{3Z}\right]\int_{-\infty}^{t}\left[\int_{0}^{1}\left(\frac{\partial K(\boldsymbol{x},t,t',s)}{\partial t'}\right)\mathrm{d}s\right]\langle \boldsymbol{u}(\boldsymbol{x},t)\boldsymbol{u}(\boldsymbol{x},t)\rangle_{t'}\,\mathrm{d}t' \tag{3.13}$$

Again, the tube survival probability, $K(\boldsymbol{x},t,t',s)$, can be determined [14] as a marginal distribution of the configuration distribution function, f, by utilizing the independence property between the process '$\boldsymbol{u}$' and the process 's'. Specifically, integrating Eq. (2.3) with respect to the process '$\boldsymbol{u}$' yields

$$\frac{DK}{Dt} = \frac{1}{\pi^2\tau_{\mathrm{d}}}\frac{\partial^2 K}{\partial s^2} - \frac{\partial}{\partial s}(\dot{s}_{\mathrm{tot}}K) - \frac{\dot{\lambda}_{\mathrm{dissip}}}{\lambda}K \tag{3.14}$$

$$K(\boldsymbol{x},t,t',s) = 1, \quad t = t' \tag{3.15}$$

$$K(\boldsymbol{x},t,t',0) = K(\boldsymbol{x},t,t',1) = 0, \quad t > 0 \tag{3.16}$$

The memory function in the expression for the polymeric stress, Eq. (3.13), can be easily determined once the above PDE for the tube survival probability, $K(\boldsymbol{x},t,t',s)$ has been solved. The details of how this PDE is solved are discussed in the next section.

To obtain the strain measure, the tube segmental orientation portion of the diffusion equation (i.e. Eq. (2.3)) must be solved. However, for the Öttinger's model this contains both, a deterministic part and

a stochastic part that arises due to the DR and CCR mechanisms

$$\frac{D\boldsymbol{u}}{Dt} = \left[\left(\boldsymbol{\delta} - \frac{\boldsymbol{uu}}{|\boldsymbol{u}|^2}\right)\cdot\boldsymbol{\kappa}\cdot\boldsymbol{u} - 2\mathcal{D}\boldsymbol{u}\right] + \sqrt{2\mathcal{D}}\left(\boldsymbol{\delta} - \frac{\boldsymbol{uu}}{|\boldsymbol{u}|^2}\right)\cdot\frac{\mathrm{d}\boldsymbol{W}}{\mathrm{d}t} \tag{3.17}$$

This equation cannot be solved analytically. Thus, the function $\langle \boldsymbol{u}(\boldsymbol{x},t,t')\boldsymbol{u}(\boldsymbol{x},t,t')\rangle$ that represents the strain measure, cannot be expressed explicitly in terms of the finger strain tensor, $\boldsymbol{B}_{t'}(\boldsymbol{x},t)$, because of the stochastic contributions due to DR and CCR. Hence, the DF method cannot be used to simulate the Öttinger's model.

However, it should be noted that in reptation models such as the "simplified" MLD model or the newly proposed MGI model, the effect of convective constraint release instead of being added as a stochastic contribution to the tube evolution equation, is taken into consideration by adding a deterministic contribution, which depends on the velocity gradient, to the reptation time scale τ_{d}. Therefore, the time evolution of the tube is totally deterministic. It is therefore straightforward to extend the DF method to such models. In fact, Peters et al. [19] and Wapperom and Keunings [22] have used the DF method to simulate complex flows of the MLD and MGI models respectively.

4. The adaptive configuration fields method

In the above summary, we have clearly shown the inadequacy of both the BCF and DF methods to simulate Öttinger's single segment reptation-based model. Specifically, the BCF method has deficiencies in dealing with the 's' variable which destroys the spatial correlation within a given field while the DF method has difficulties with the '$\boldsymbol{u}$' variable, which arises from the fact that the strain measure is stochastic. In fact the problem encountered by DF method arises in many kinetic theory-based models (e.g. rigid dumbbell model [28], Curtiss–Bird model [28]) which have diffusion effects/Brownian motion in the part governing the orientation of the kinetic species. As in the Öttinger's model, it is not possible to get a closed form solution to these equations unless perturbation methods are used and the stress equation is formulated in the form of a retarded motion expansion. Although retarded motion expansions are a powerful tool in producing the linear viscoelastic properties and viscometric functions at low Weissenberg numbers, they cannot be extended to flows with O(1) Weissenberg numbers. Hence, in order to simulate flow of this class of models in complex geometries and O(1) Weissenberg numbers, one needs to explore new strategies. In what follows we will describe a new technique, namely, "the adaptive configuration fields method" that allows simulation of this class of models in complex kinematics flows.

The stress equation for the Öttinger model is given by Eq. (3.13). To obtain the stress, one needs to determine $\lambda(\boldsymbol{x},t)$, $K(\boldsymbol{x},t,t',s)$ and $\boldsymbol{u}(\boldsymbol{x},t)$. The treatment of the stretch variable is discussed in Section 3. Specifically, the evolution of the chain stretch is determined by solving Eq. (3.4) along with the initial condition, Eq. (3.5). The determination of the tube survival probability, $K(\boldsymbol{x},t,t',s)$, requires the solution to the PDE, Eq. (3.14), along with the initial condition Eq. (3.15) and the boundary conditions Eq. (3.16). In general, one cannot obtain a closed form solution to this equation. However, if one invokes a pseudo steady-state approximation (i.e. the variable λ is assumed to be constant and equal to the present value of the chain stretch, $\lambda = \lambda(t)$), one can easily obtain a closed form solution to the above PDE in a self consistent manner by the method of eigen function expansions. Appendix A outlines the derivation of the solution using this approximation. The use of the concept of a pseudo steady-state approximation in transient simulations requires justification. However, it should be noted that the error associated with this

Table 1
"Simplified" Mead–Larson–Doi [15] equation set

Stretch	$\frac{\partial\lambda}{\partial t} = \lambda\boldsymbol{\kappa} : \boldsymbol{\tau} - \frac{2}{\tau_s}\frac{\lambda[\lambda-1]}{[\lambda+1]}$
Orientation tensor	$\boldsymbol{\tau} = \int_{-\infty}^{t}\frac{dt'}{\tau(t')}\exp\left[-\int_{t'}^{t}\frac{dt''}{t''}\right] g[\boldsymbol{B}_{t'}(t)]$
Strain measure	$g[\boldsymbol{B}_{t'}(t)] = \left\langle \frac{\boldsymbol{B}_{t'}^{1/2}(t)\cdot\boldsymbol{u}(t')\boldsymbol{B}_{t'}^{1/2}(t)\cdot\boldsymbol{u}(t')}{\lvert\boldsymbol{B}_{t'}^{1/2}(t)\cdot\boldsymbol{u}(t')\rvert^2}\right\rangle_{t'}$
Relaxation time	$\frac{1}{\tau} = \frac{1}{\lambda^2\tau_d} + \frac{1}{\lambda}\left[\frac{2}{\tau_s}\frac{(\lambda-1)}{(\lambda+1)}\right]$
Stress	$\boldsymbol{\tau} = 5G_N^0\lambda^2\boldsymbol{\tau}, \quad G_N^0 =$ plateau modulus

approximation is very small, due to the exponential nature of solution of the tube survival probability, $K(s,t,t')$. To prove that this error is indeed very small, we have performed simulations with the "simplified" MLD model [15]. The equation set for this model is listed in Table 1. Invoking the pseudo steady-state approximation, for the memory function for this model results in the following modified form of the orientation tensor expression:

$$\boldsymbol{\tau} = \frac{1}{\tau(t)}\int_{-\infty}^{t} dt' \exp\left[-\frac{(t-t')}{\tau(t)}\right] g[\boldsymbol{B}_{t'}(t)] \tag{4.1}$$

Figs. 1 and 2 show the transient shear and uniaxial elongational flow simulation results for the "simplified" MLD using the above orientation tensor expression. Also shown in these figures are the simulation results with the exact orientation tensor expression as given in Table 1. The difference between these transient simulation results is <0.01% for the startup of steady shear and <10% for the startup of steady uniaxial elongational flow. Clearly, this proves the validity of the pseudo steady-state

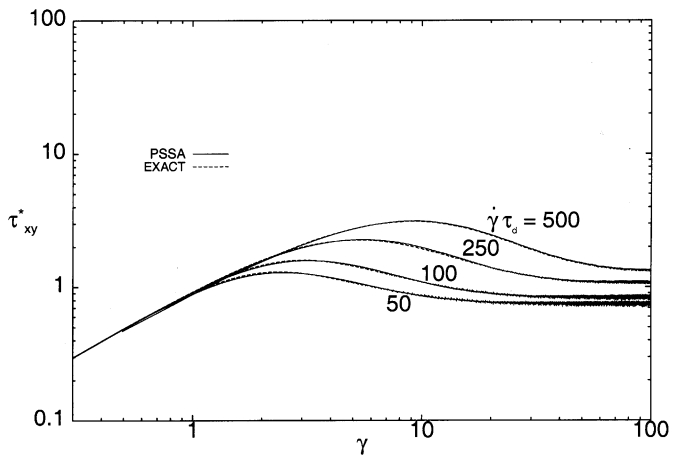

Fig. 1. Comparison of the simulation results for startup of steady shear flow using the memory function employing pseudo steady-state assumption (PSSA) with the results using the EXACT memory function, for the "simplified" Mead–Larson–Doi model. $\tau^*_{xy} = (\tau_{xy}(t)/G_N^0)$, $\gamma = \dot{\gamma}t$ is the shear strain and $(\tau_d/\tau_s) = 50$.

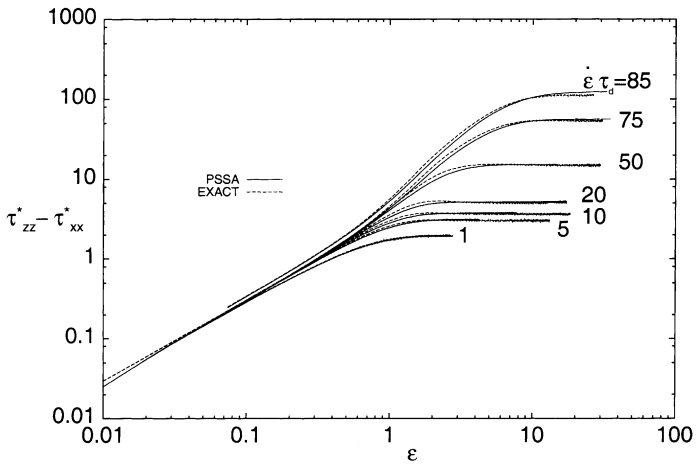

Fig. 2. Comparison of the simulation results for the startup of steady uniaxial elongational flow using the memory function employing pseudo steady-state assumption (PSSA) with the results using the EXACT memory function, for the "simplified" Mead–Larson–Doi model. $\tau^*_{zz} - \tau^*_{xx} = (\tau_{zz}(t) - \tau_{xx}(t)/G^0_N)$, $\varepsilon = \dot{\boldsymbol{\epsilon}}t$ is the elongational strain and $(\tau_d/\tau_s) = 50$.

approximation employed. Later we arrive at the same conclusion for the Öttinger's model as well thus verifying the generic applicability of this approach.

Using the above strategies we can determine both λ and $K(s, t, t')$, hence, once the orientation, $\boldsymbol{u}(x, t)$, is determined the polymeric stress can be computed. Since the tube segmental orientation is not deterministic and perturbation solutions for the SDE governing the segmental orientation is limited to small Weissenberg numbers, it is not possible to relate the initial and the final tube orientation with an explicit equation and one has to track the tube evolution. However, as mentioned in Section 3, the BCF method can be effectively used to track the tube evolution by using Eq. (3.6). Hence, we will solve this SDE using Brownian dynamics to obtain the tube evolution and the strain measure at the present time, t. Specifically, the strain required in the stress expression, Eq. (3.13), is computed by propagating 'N' configuration fields, as in the BCF method, each of which is governed by the Eq. (3.6) with the initial condition being that each field at the time of its birth is a spatially uniform random unit vector chosen from the isotropic distribution on the surface of a unit sphere. The 'N' configuration fields are segregated into 'M' parts, each carrying 'N/M' fields individually. These 'M' parts are the representation of the ensembles which were born at different times t' in the past. The 'N/M' fields within each ensemble are referred to as sub-ensembles and it is actually the simulation of these sub-ensembles that is being performed when one evolves the 'N' configuration fields.

The 'N' configuration fields that we use however, have important differences from the ones used in the BCF method. The first and perhaps the most important difference is that unlike the BCF method, the configuration fields used in our approach, have a fixed lifetime, and it is only during their lifetime that we make use of them in calculating the strain measure. This procedure is very similar to the DF method, where the deformation gradient fields, $\boldsymbol{B}_{t'}(\boldsymbol{x}, t)$, have a fixed lifetime. Therefore, as shown in the DF method, keeping very old fields is a waste of resources and here too we would adaptively create and destroy fields according to our need.

The second important difference between the BCF method and the "adaptive configuration fields" is that random walkers are not attached to the fields. The important thing to realize at this stage is that, the

purpose of the random walker is to decide the age of the tube, but in our approach, the age is decided by explicitly solving for the tube survival probability $K(\boldsymbol{x}, t, t', s)$ in the same way as in the DF method. Note that this probability is a function of the stretch field, $\lambda(\boldsymbol{x}, t)$, and therefore the life of the tube varies spatially.

In what follows, we briefly discuss the algorithm for the computer implementation of the adaptive configuration fields method.

4.1. Governing equations/computational methodology

The temporal discretization of the stretch field evolution equation, Eq. (3.4), is obtained through a forward Euler scheme which results in the following update of the stretch field from time $t_n = n\Delta t$ to time $t_{n+1} = (n+1)\Delta t$:

$$\lambda^{n+1}(\boldsymbol{x}, t) + (\boldsymbol{v}^n(\boldsymbol{x}, t) \cdot \nabla\lambda^{n+1}(\boldsymbol{x}, t))\Delta t = \lambda^n(\boldsymbol{x}, t) + (\dot{\lambda}^n_{\text{conv}}(\boldsymbol{x}, t) + \dot{\lambda}^n_{\text{dissip}}(\boldsymbol{x}, t))\Delta t \tag{4.2}$$

where,

$$\dot{\lambda}^n_{\text{conv}}(\boldsymbol{x}, t) = \lambda^n(\boldsymbol{x}, t)\boldsymbol{\kappa}^n(\boldsymbol{x}, t) : \boldsymbol{\tau}^n(\boldsymbol{x}, t) \tag{4.3}$$

$$\dot{\lambda}^n_{\text{dissip}}(\boldsymbol{x}, t) = -\frac{1}{\tau_s}\frac{c(\lambda^n(\boldsymbol{x}, t))}{3Z}(\lambda^n(\boldsymbol{x}, t) - 1) \tag{4.4}$$

The configuration fields evolution equation, i.e. Eq. (3.6), is discretized using a forward Euler scheme, which preserves the unit norm property of the tube orientation vector

$$\boldsymbol{u}'_k(\boldsymbol{x}, t) + (\boldsymbol{v}^n(\boldsymbol{x}, t) \cdot \nabla\boldsymbol{u}'_k(\boldsymbol{x}, t))\Delta t = \boldsymbol{u}^n_k(\boldsymbol{x}, t) + \boldsymbol{\kappa}^n(\boldsymbol{x}, t) \cdot \boldsymbol{u}^n_k(\boldsymbol{x}, t)\Delta t + \sqrt{2\mathcal{D}^n(\boldsymbol{x}, t)}\Delta\boldsymbol{W} \tag{4.5}$$

$$\boldsymbol{u}^{n+1}_k(\boldsymbol{x}, t) = \frac{\boldsymbol{u}'_k(\boldsymbol{x}, t)}{|\boldsymbol{u}'_k(\boldsymbol{x}, t)|} \tag{4.6}$$

Next, in order to obtain the strain measure, $\langle \boldsymbol{u}(\boldsymbol{x}, t)\boldsymbol{u}(\boldsymbol{x}, t)\rangle_{t'}$, we make use of the algorithm developed in the original DF method [21]. Specifically, sampling of the orientation of tubes is performed at a finite number of the times, 'M', in the history and the strain measure is obtained by a continuous linear interpolation between these sampled values (see Fig. 3),

$$\langle \boldsymbol{u}(\boldsymbol{x}, t)\boldsymbol{u}(\boldsymbol{x}, t)\rangle_{t'} = \sum_{k=0}^{M-1} \langle \boldsymbol{u}(\boldsymbol{x}, t)\boldsymbol{u}(\boldsymbol{x}, t)\rangle_{t'_k}\phi_k(t') \tag{4.7}$$

where, $\phi_k(t')$ are the piece-wise linear top hat shape functions, which have life only over the time interval $[t'_{k-1}\ t'_{k+1}]$ and t'_k are the times in the history at which one carries out the sampling. In the above formulation a cutoff time, τ_c, is also needed to restrict the reference time to $t - \tau_c < t' < t$. This limits the number of intervals to 'M' and hence the strain measure is easily calculated as a finite sum, Eq. (4.7). The 'M' ensembles carrying the 'N' fields introduced earlier, are attached individually with the 'M' time intervals. Moreover, each of these intervals is further divided into a number of equidistant steps each equal to the simulation time step size of Δt. The sub-intervals formed serve as position levels for the ensembles during their lifetime, so that at every time step the ensembles age by Δt and their position gets updated to the next lower sub-interval.

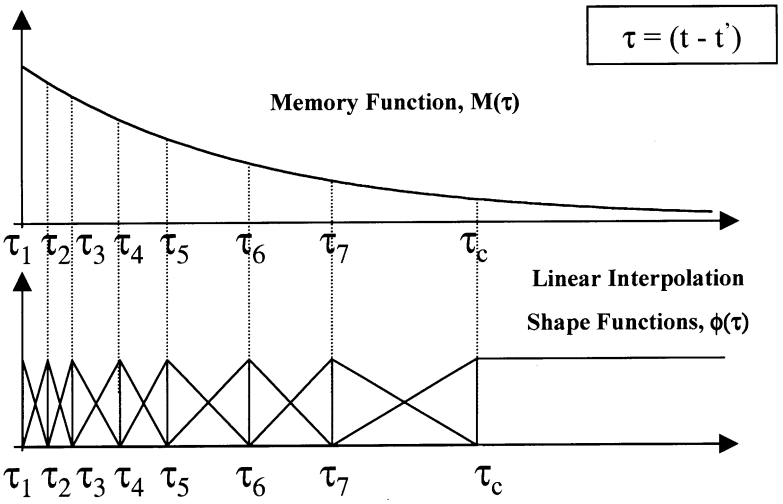

Fig. 3. A typical memory function for the Öttinger's model and its discretization using linear interpolation shape functions.

Since the memory function for the Öttinger model typically decreases exponentially with increasing time, sampling is performed with unequal time steps, as shown in Fig. 3, in such a way that at selected time instances the interval length gets doubled, so that finally a fine time mesh partitioning results near the present time, $t = t'_0$, where the memory function changes rapidly and an increasingly coarse discretization is obtained, as one proceeds into the history of the flow, where the memory function varies slowly. Specifically, the following discretization, suggested in [18], is used: starting with the present time, we use 25 intervals of Δt, followed by 25 intervals of $2\Delta t$, 10 intervals of $4\Delta t$, 10 intervals of $8\Delta t$, 10 intervals of $16\Delta t$, 10 intervals of $32\Delta t$, 10 intervals of $64\Delta t$, 10 intervals of $128\Delta t$, 10 intervals of $256\Delta t$, 10 intervals of $512\Delta t$ and finally 10 intervals of $1024\Delta t$. With this memory discretization the total number of ensembles to be used is $M = 140$ and with a $\Delta t = 0.0001\pi^2\tau_d$ (a typical value used in our simulations), the cutoff time, τ_c comes out to be of a sufficiently large value of approximately $20\tau_d$. It is possible to change the cutoff time, τ_c, by varying the Δt and/or by changing the number of ensembles (and hence the number of time intervals). Thus with this description, the sub-ensemble size, 'N/M', the number of ensembles, 'M', and the time step, Δt, constitutive the parameters of the simulations. These issues will be discussed in the next section.

The above approach thus limits the amount of information to be processed such that the propagation of only M ensembles, which store the information on the strain measure at finite discrete reference times, t'_k, is sufficient for calculating the strain measure, $\langle \boldsymbol{u}(\boldsymbol{x}, t)\boldsymbol{u}(\boldsymbol{x}, t)\rangle_{t'}$, at 'all' the reference times, t'. For a more detailed discussion on this subject we refer the reader to the original paper by Peters et al. [21].

Substitution of Eq. (4.7) into Eq. (3.13) results in replacement of the time integral in the stress expression, Eq. (3.13), with a finite sum

$$\frac{\boldsymbol{\tau}(\boldsymbol{x}, t)}{3Zn_p k_B T} = \left[1 + \frac{c(\lambda(\boldsymbol{x}, t))\lambda(\boldsymbol{x}, t)(\lambda(\boldsymbol{x}, t) - 1)}{3Z}\right] \sum_{k=0}^{M-1} W_k \langle \boldsymbol{u}(\boldsymbol{x}, t)\boldsymbol{u}(\boldsymbol{x}, t)\rangle_{t'_k} \tag{4.8}$$

where the weights, W_k, are given by

$$W_k = \int_{-\infty}^{t} \left[\int_0^1 \left(\frac{\partial K(\boldsymbol{x}, t, t', s)}{\partial t'} \right) \mathrm{d}s \right] \phi_k(t') \, \mathrm{d}t', \quad k = 0, 1, 2, \ldots, M-1 \tag{4.9}$$

A typical simulation starts with 'N' spatially uniform unit vector fields, $\boldsymbol{u}_{\mathrm{k},0}$, chosen from the isotropic distribution on the surface of a unit sphere. The 'N' fields, as discussed earlier, are segregated into 'M' ensembles and these ensembles are assigned to the 'M' time intervals of the memory integral discretization. The simulation proceeds using the forward Euler scheme with time steps of Δt. In accordance with the original DF algorithm [21] where the deformation fields are evolved and later destroyed at a certain age, at every time step, the 'ensembles' are evolved, assigned the right age, and then selectively destroyed at a certain age. At the same time, to keep the number of ensembles fixed at 'M', a new ensemble, with 'N/M' spatially uniform fields, is introduced in the simulation which takes the place of the discarded ensemble. Such a procedure ensures that the aged ensembles, which contribute negligibly to the overall stress at the present time, 't', are not unnecessarily evolved in the simulation and at the same time the ensembles born recently, which have large contributions to the stress, are easily incorporated in the fixed limited memory available. The remaining 'N–(N/M)' fields in the rest of the undiscarded ensembles get updated every time step according to Eqs. (4.5) and (4.6). Also, the stretch field, $\lambda(\boldsymbol{x}, t)$, is updated according to Eqs. (4.2)–(4.4). Finally, the weights required in the stress expression are computed using the tube survival probability, $K(\boldsymbol{x}, t, t', s)$ in the weight expression, Eq. (4.9). The weights depend on the stretch variable $\lambda(\boldsymbol{x}, t)$ and so here unlike in the Doi–Edwards model, they are a function of both time and space. Therefore, one needs to compute these weights at every time step and every spatial location. Assembling this information together with the velocity gradient tensor, one can easily calculate the polymeric stress using Eq. (4.8). This procedure is demonstrated in the next section.

5. Results and discussion

In order to fully examine the fidelity and robustness of our new simulation technique, we have simulated the Öttinger's model in a number of different fixed kinematics flows. For such flows the velocity gradient tensor has no spatial variations and is known explicitly. Hence, pure Brownian dynamics simulations can be easily performed to obtain the polymeric stress. In turn, these results can be used for validation of our newly proposed ACFM method. Motivated by earlier theoretical and experimental studies, for all of our simulations we take the following parameter values [6,7,15]: $Z = 7$, $\lambda_{\max} = 21$, $\delta_1 = \delta_2 = 1/\lambda$ and $\tau_{\mathrm{d}}/\tau_{\mathrm{s}} = 3Z$.

For pure Brownian dynamics simulations, we use the simulation algorithm suggested by Fang et al. [7]. Specifically, a large number (N_{sample}) of trajectories are propagated for the stochastic processes, $\boldsymbol{u}_t$ and s_t, which are governed by the SDEs, Eqs. (2.8) and (2.9). At the same time the stretch variable, λ, is evolved by utilizing Eqs. (2.1) and (2.2). Finally, to achieve a full equivalence with the diffusion equation, Eq. (2.3), the creation/destruction term, $\dot{\lambda}_{\mathrm{dissip}} f/\lambda$, which is absent in the SDEs, is taken into consideration in a probabilistic manner after observing the net flux of configurations in and out of the interval [0,1]. Using this procedure, the simulation proceeds with a forward Euler scheme in time steps of Δt and the stress at any time, t, is easily evaluated by taking an ensemble average over the trajectories (Eq. (2.10)). To ensure convergence, in all of our simulations we have chosen (after several trial and error procedures with different ensemble sizes and time steps) a sufficiently large ensemble size of $N_{\mathrm{sample}} = 100{,}000$ and a

Table 2
Sample lookup-table. The memory integral discretization is as explained in Section 4.1 and the sub-interval size is $\Delta t = 0.0001\pi^2\tau_d$

λ	W_0	W_1	W_2	W_3	W_4
1.0000	0.015062	0.012447	0.008114	0.006561	0.005664
1.0156	0.014907	0.012142	0.007815	0.006267	0.005373
1.0312	0.014880	0.011737	0.007537	0.005994	0.005104
1.0625	0.014609	0.011215	0.007033	0.005503	0.004624
1.1250	0.014145	0.010337	0.006202	0.004706	0.003854
1.2500	0.013482	0.009019	0.005036	0.003619	0.002829
1.5000	0.012638	0.007505	0.003758	0.002485	0.001807

small enough time step size of $\Delta t = 0.0001\pi^2\tau_d$. As a further step in performing efficient calculations, we make use of the improved higher order (i.e. $O(\Delta t)$) scheme of Öttinger [29], which takes into account the unobserved reflections (i.e. the cause of lower order (i.e. $O(\sqrt{\Delta t})$) convergence of the conventional Euler scheme) through a conditional probability of their occurrence. Finally, in order to compute the statistical errors for the results, we have performed 10 independent simulations. For all the pure Brownian dynamics results which we use for comparison purposes later, the statistical errors are less than $\pm 0.1\%$.

The ACFM calculations are performed using the computational methodology outlined in the previous section (see Eqs. (4.2) through (4.9)). It should be noted that since we have performed simulations for unidirectional fully developed flows, the material convection terms in the ACFM equations conveniently drop out. A use of this fact becomes immediately obvious when it is observed that the PDE, Eq. (3.14), governing tube survival probability, $K(t, t', s)$, under the assumption of pseudo steady state, has only a single parameter, λ, which itself is restricted to $\lambda \leq \lambda_{max}$. Therefore, the solution of this PDE (and hence of the resulting costly eigen value problems) could thus be easily obtained beforehand for all values of $\lambda \leq \lambda_{max}$ and the weights, W_k. Hence, one can obtain the stress expression, Eq. (4.8) from the simulations. We use this strategy as an efficient way of performing our ACFM time integration simulations. Before the actual simulation starts, the PDE is solved spanning the whole λ parameter space in discrete values differing by $\Delta\lambda = 0.001$, and the weights are computed using this solution in order to generate 'lookup-tables' for these discrete values. A sample lookup-table containing the first few weights for some discrete values of the stretch variable (λ) is presented as Table 2. During the course of the simulations, depending upon the actual stretch variable value, the required weights are obtained by interpolating between those values from the 'lookup-tables' which were obtained for the immediate lower (λ_l) and upper (λ_u) discrete values of λ ($\lambda_l \leq \lambda \leq \lambda_u$). Such an approach thus significantly affects the computational efficiency of the simulations. Typically a 100% reductions in CPU time are observed with the use of lookup-tables.

As a step further in increasing the computational efficiency of our technique, we have examined the sub-ensemble generation process. Isotropically distributed sub-ensembles are required both at the start of the simulation and during the course of simulation at the time of replacement of an old ensemble with a new one. As shown by van Heel et al. [18], a small sized ensemble having evenly distributed sub-ensemble vectors can easily outperform the results obtained by calculations with a relatively large sized ensemble having randomly distributed sub-ensembles. This is due to the fact that an isotropic even distribution constitutes an unbiased initial tube configuration space and is thus able to accurately capture the deformation experienced by the ensemble later. Hence, for all our simulations we have used ensembles

with homogeneously distributed sub-ensemble unit vectors. Such a choice not only gives better results with fewer degrees of freedom, but even offers an additional advantage of further CPU time reduction, since now each subsequent ensemble generation is easily achieved by a single random rotation of the very first ensemble, hence avoiding the excessive use of costly random number generation processes which are an integral part of the conventional randomly distributed ensemble generation algorithms. The random numbers which are still needed for the generation of Wiener processes and for the random rotations, are obtained by using highly efficient routines based on Lagged Fibonacci Sequences [30]. The above procedure typically results in an additional 20% relative reduction in CPU time.

Next, one needs to determine the optimum sub-ensemble size, 'N/M', the number of ensembles, 'M', and the time step size, Δt, which is done by performing numerical experiments. In accordance with the theoretical predictions, the error bars are seen to be inversely proportional to the square-root of the sub-ensemble size. The exact convergence criterion with respect to the number of ensembles and the time step size is however not easy to establish since a combination of both parameters determines how well one can capture the initial steep behavior of the memory function as well as the final cutoff time. It therefore becomes difficult to vary either the number of ensembles or the time step size independent of the other and still extract the information on how well the memory function is approximated. However, due to the stochastic nature of the equations being integrated, the error varies as $\sqrt{\Delta t}$ and typically a time step size of $\Delta t = 0.0001\pi^2\tau_d$ was found to be appropriate for converged results. Hence, we have used this value for all of our ACFM simulations. Similarly, appropriate values for the number of ensembles, 'M', and the sub-ensemble size, 'N/M', were obtained. For example, in the startup of steady shear flow, at a dimensionless shear rate of $\dot{\gamma}\tau_d = 10$, ($M = 130$) ensembles with a sub-ensemble size of ($N/M = 40$) were observed to be sufficient, so that the total number of configuration fields needed for this simulation was $N = 130 \times 40 = 5200$. Figs. 4 and 5 show the convergence results for these trial

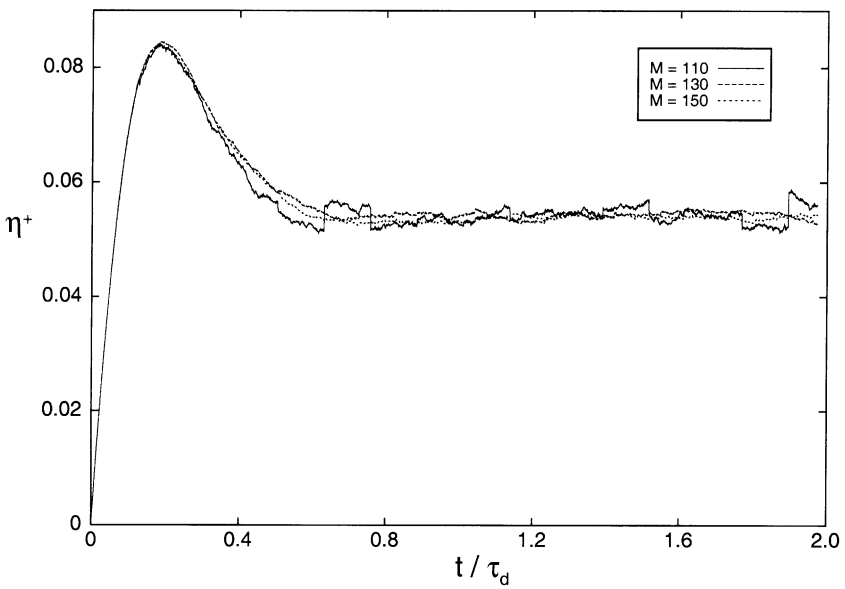

Fig. 4. The convergence characteristics of the adaptive configuration fields method (ACFM) in terms of the number of ensembles, M, used. $\dot{\gamma}\tau_d = 10$ and $\eta^+ = (5\tau_{xy}(t)/3Zn_pk_BT(\dot{\gamma}\tau_d))$ is the transient viscosity in the startup of the steady shear flow.

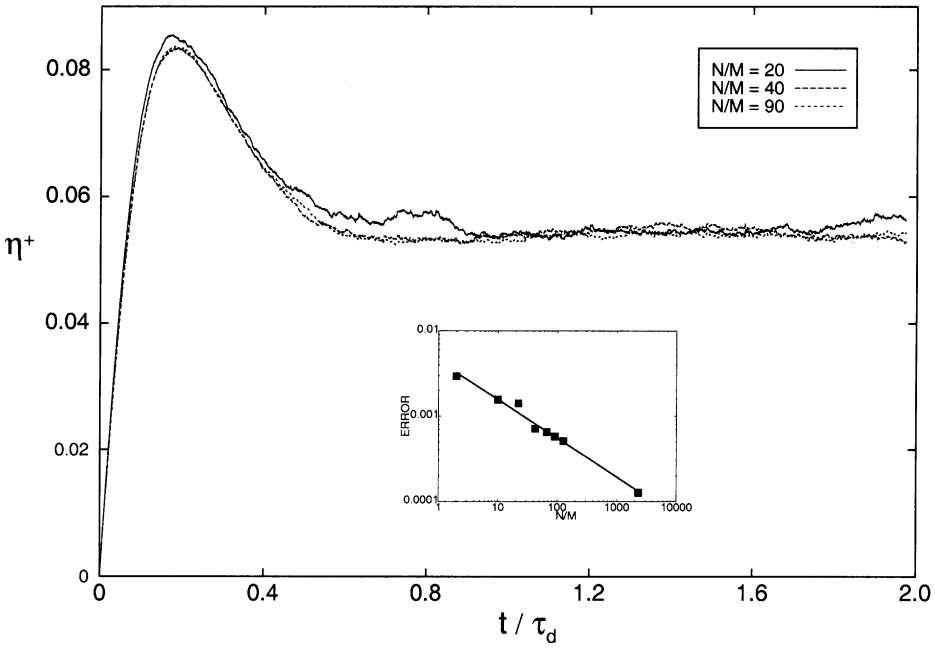

Fig. 5. The convergence characteristics of the adaptive configuration fields method (ACFM) in terms of the sub-ensemble size, N/M, used in each of the M ensembles. $\dot{\gamma}\tau_d = 10$ and $\eta^+ = (5\tau_{xy}(t)/3Zn_p k_B T(\dot{\gamma}\tau_d))$ is the transient viscosity in the startup of the steady shear flow. The inset has the log–log plot of the statistical error versus the sub-ensemble size. Also shown in the inset is the fit of the error to a linear function of $\left(1/\sqrt{N/M}\right)$.

simulations using transient viscosity as the measured variable. The $M = 110$ case highlights the fact that the resulting cutoff time ($\tau_c \approx 2.6\tau_d$) is clearly not enough. In other words, the weight associated with the last ensemble, in this case, is still considerably large to be neglected. However, for the $M = 130$ and 150 case, the resulting τ_c is approximately 10 and $40\tau_d$, respectively which is more than sufficient. The inset of Fig. 5 shows the inverse square-root dependence on the sub-ensemble size. These figures are a representation of the fact that convergence can be obtained using a reasonable finite number of ensembles and sub-ensembles. In general, as the dimensionless shear rate increases, larger number of ensembles with increased sub-ensemble size are needed.

Again, as in the pure Brownian dynamics simulations, the statistical error bars for the computed results are obtained by performing 10 independent simulations. For all the simulation results which we present in this paper, the errors are less than ±0.1%.

5.1. Startup of steady shear flow

The first test problem considered was that of startup of steady shear flow. Figs. 6 and 7 show our simulation results for the dimensionless transient viscosity and the dimensionless transient first normal stress coefficient respectively for various values of the dimensionless shear rate $\dot{\gamma}\tau_d$. For purpose of comparison, these figures also include the corresponding data from pure Brownian dynamics simulations. Clearly our newly proposed adaptive configuration fields method fully captures the intricate non-linear

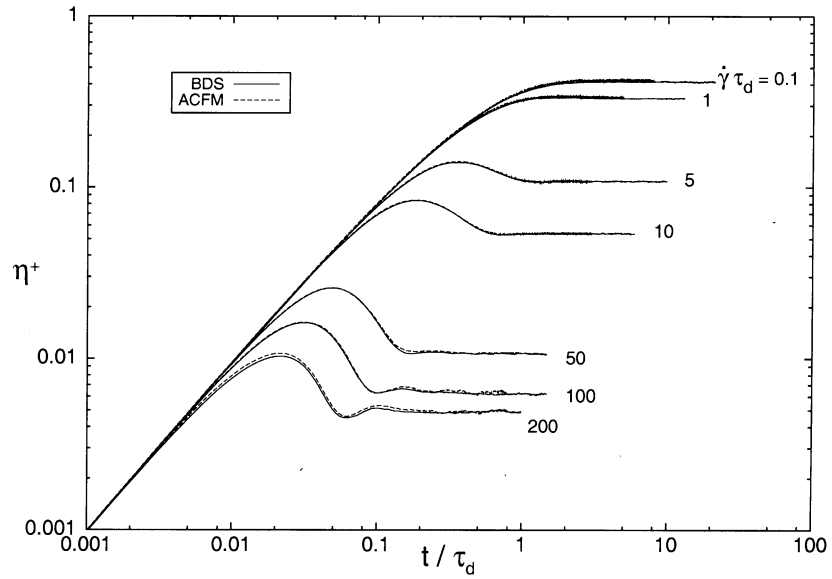

Fig. 6. Comparison of the Brownian dynamics simulation (BDS) results with adaptive configuration fields method (ACFM) results using transient viscosity, $\eta^+ = (5\tau_{xy}(t)/3Zn_pk_BT(\dot{\gamma}\tau_d))$ in the startup of the steady shear flow as the measured variable.

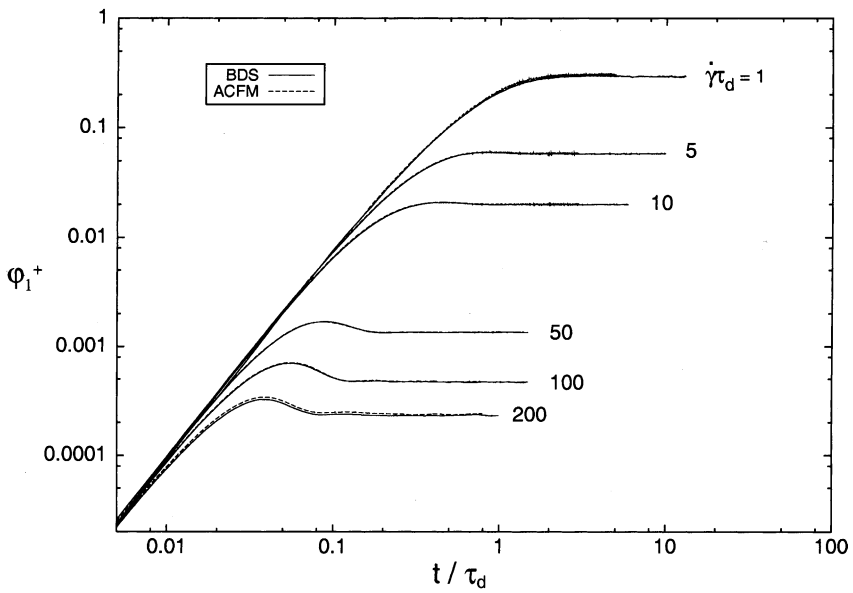

Fig. 7. Comparison of the Brownian dynamics simulation (BDS) results with adaptive configuration fields method (ACFM) results using transient first normal stress coefficient, $\psi^+ = (5(\tau_{xx}(t) - \tau_{yy}(t))/3Zn_pk_BT(\dot{\gamma}\tau_d)^2)$ in the startup of steady shear flow as the measured variable.

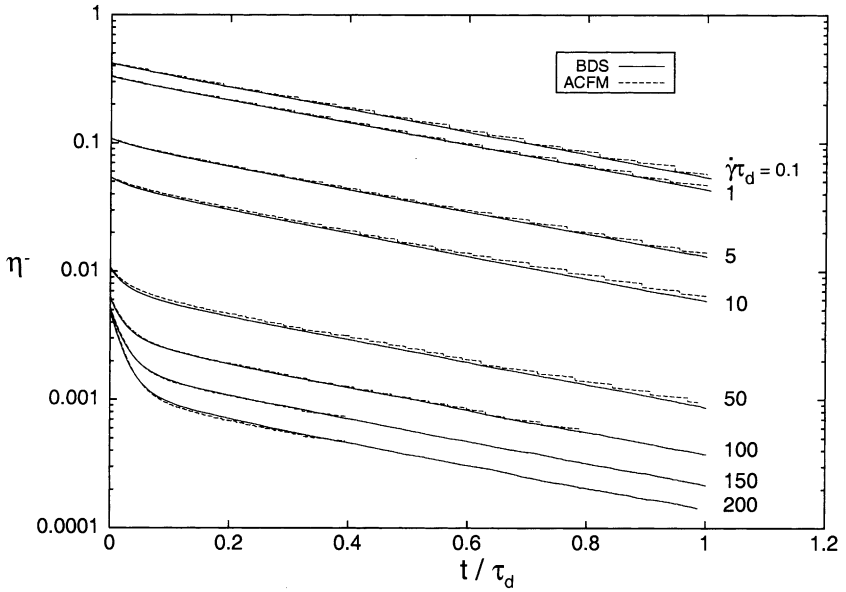

Fig. 8. Comparison of the Brownian dynamics simulation (BDS) results with adaptive configuration fields method (ACFM) results using transient viscosity, $\eta^- = (5\tau_{xy}(t)/3Zn_p k_B T(\dot{\gamma}\tau_d))$ in the cessation of the steady shear flow as the measured variable.

shear rheology of the entangled polymers and a very good agreement is obtained with the pure Brownian dynamics simulation results.

5.2. Cessation of steady shear flow

The next problem considered was that of cessation of steady shear flow. Figs. 8 and 9 show the relaxation of stresses after the flow is switched off. Specifically, Fig. 8 shows the transient dimensionless viscosity and Fig. 9 shows the transient dimensionless first normal stress coefficient. As expected, the stress shows a steady exponential decrease with time. Again, the results from the two simulations are very close to each other. However, a close examination of the ACFM results reveals periodical jumps. These jumps can be easily associated with the temporal discretization involved. Note that such jumps follow a trend (a geometric progression) which is closely related to the memory integral discretization used (Section 4.1). In other words, since the ensemble that disappears at any instant, *t*, can be quite young and since the new ensemble that takes its place has a zero contribution to the stress at that instant, a significant portion of the stress is lost at such instances. This phenomenon is thus an integral part of the temporal discretization employed and gets clearly highlighted in slow flows such as cessation or startups at low shear rates as opposed to fast flows where the combined *new* contribution from the other ensembles is large enough to maintain the continuity that is being compromised from the zero contribution of the new ensemble.

5.3. Uniaxial extensional flow

As a final verification of our technique, the uniaxial extensional flow problem was simulated. Fig. 10 shows the transient uniaxial viscosity observed during the simulation of startup of uniaxial extensional

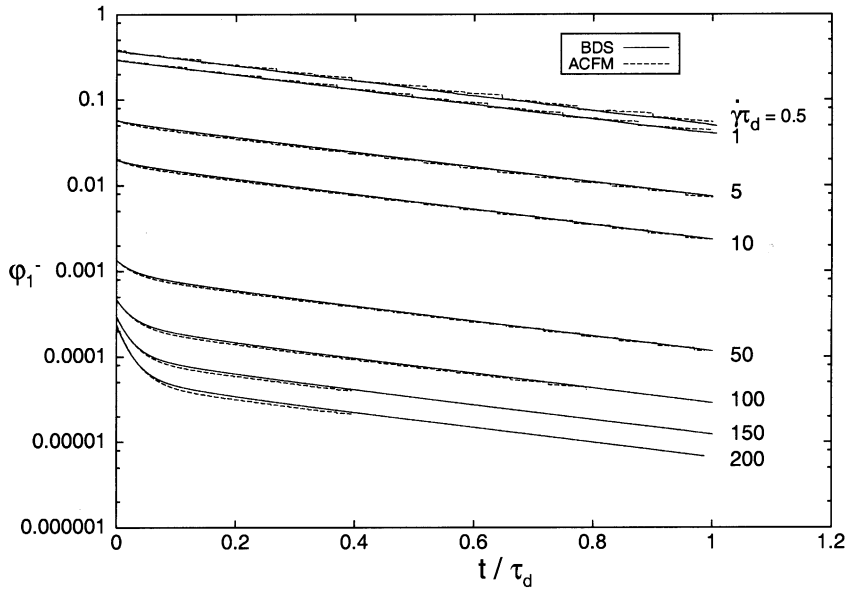

Fig. 9. Comparison of the Brownian dynamics simulation (BDS) results with adaptive configuration fields method (ACFM) results using transient first normal stress coefficient, $\psi^- = (5(\tau_{xx}(t) - \tau_{yy}(t))/3Zn_p k_B T(\dot{\gamma}\tau_d)^2)$ in the cessation of the steady shear flow as the measured variable.

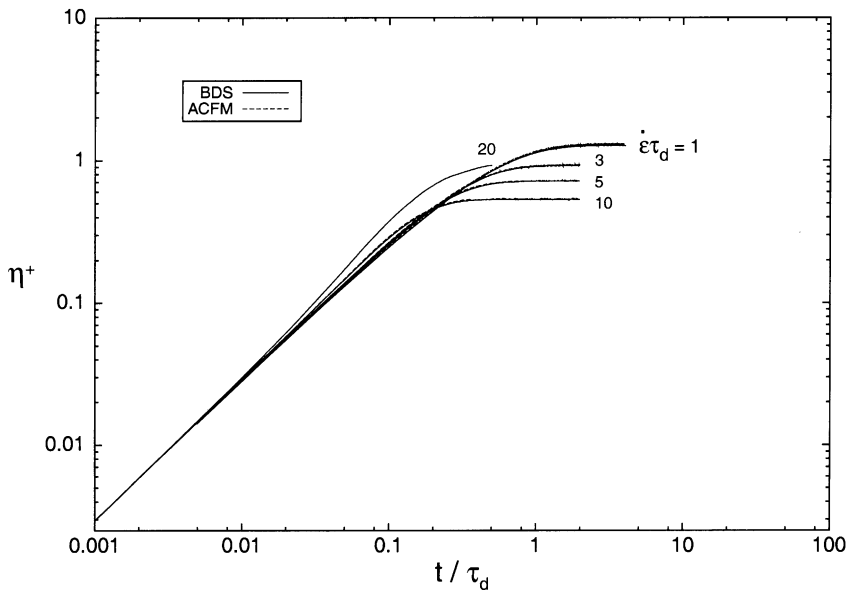

Fig. 10. Comparison of the Brownian dynamics simulation (BDS) results with adaptive configuration fields method (ACFM) results using transient viscosity, $\eta^+ = (5(\tau_{zz}(t) - \tau_{xx}(t))/3Zn_p k_B T(\dot{\varepsilon}\tau_d))$ in the startup of the steady uniaxial extensional flow as the measured variable.

flow. The flow has been simulated for various values of dimensionless extension rate, $\dot{\varepsilon}\tau_d$. Clearly, the ACFM simulations can accurately capture the relevant dynamics.

6. Conclusions

In recent years, a number of sophisticated models based on the concept of reptation have been developed for describing the non-linear rheology of entangled polymeric systems [7,13,15]. In order to incorporate these models in complex flow simulations, new efficient simulation strategies are required. We have developed a new multiscale Eulerian technique, i.e. the adaptive configuration fields method, that allows complex flow simulation of advanced reptation models with stochastic strain measures and local variations of life span distribution. This technique is a new hybrid method that carefully avoids the drawbacks of the state-of-the-art Eulerian techniques for multiscale simulation of entangled polymeric systems, namely, the Brownian configuration fields [20] and the deformation fields [21] methods. To demonstrate the fidelity and robustness of our method, we have simulated the Öttinger's single segment reptation model in a number of fixed kinematics flows and obtained a one-to-one correspondence with the pure Brownian dynamics simulations, thus verifying the accuracy of our method.

A comparison of the CPU times between ACFM and pure Brownian dynamics BD has also been performed and it was found that the ACFM simulations are typically more CPU intensive than the BD simulations. This is because in the ACFM calculations the total number of configuration species (N) required is more than the total number of trajectories (N_{sample}) needed in BD simulations. For example, at a dimensionless shear rate of $\dot{\gamma}\tau_d = 10$, if one requires the statistical error for the simulation to be less than $\pm 0.03\%$, the total number of configuration fields needed in the ACFM calculations is about $N = 300{,}000$ (with 150 ensembles of sub-ensemble size equal to 2000), whereas in BD simulations the total number of trajectories required is about $N_{\text{sample}} = 100{,}000$, which makes the BD simulations in this case approximately three times faster than the ACFM simulations. However, it has to be noted that in the current implementation of the ACFM technique discussed here, a fixed sub-ensemble size is assigned to each ensemble member irrespective of its age, which implies that even the younger ensembles, which have a larger contribution to the instantaneous stress, are calculated within the same statistical accuracy as the older ensembles which contribute in a small proportion to the instantaneous stress. Hence, in order to obtain a lower overall statistical error, the total number of trajectories to be employed is sufficiently high. On the other hand, this problem doesn't exist for the BD simulations where such a sorting procedure is never required since the age of the kinetic species (trajectories) is decided implicitly by the 'reflection' procedure, and hence, a smaller trajectory size is sufficient for reasonable accuracy. However, it should also be noted that the use of Brownian dynamics in complex flow simulations requires a coupling with particle tracking Lagrangian techniques which makes the overall simulation strategy more computationally intensive as compared to the Eulerian ACFM technique.

Nonetheless, one can also improve the efficiency of the ACFM technique per se by adaptively decreasing the sub-ensemble size assigned to the older ensembles. We have modified the ACFM implementation suggested here to include an algorithm that appropriately fixes the sub-ensemble size for the ensembles present. Starting with a sufficiently high value, sub-ensemble size for the following ensembles is adaptively decreased in accordance with the weights. Using such a procedure further reduction in the simulation CPU time has been proved to be possible, both in fixed kinematics and in complex flows and one obtains similar computational efficiency as the Brownian dynamics for the case of fixed kinematics flows

Table 3
Comparison of the simulation CPU time (in minutes) of pure Brownian dynamics (BDS) with the adaptive sub-ensemble size ACFM method

	$N_{traj} = 101{,}200$	$N_{traj} = 121{,}000$	$N_{traj} = 140{,}800$	$N_{traj} = 160{,}600$
BDS	4.16	4.97	6.01	6.66
ACFM	4.22	5.01	6.09	6.73

All computations have been performed for the case of startup of steady shear flow at $\dot{\gamma}\tau_d = 10$, on a 667 MHz Alpha system with 2GB memory. With a time step size of $\Delta t = 0.0001\pi^2\tau_d$, 2000 time steps are required to reach the steady state. N_{traj} is the total number of trajectories used.

(see Table 3.). We have also tried to use higher order shape functions to approximate the memory function in our ACFM method. However, we have found that such refinements increase the computational cost tremendously without producing significant changes in terms of accuracy or efficiency of the method.

Acknowledgements

This work has been supported by a grant from the National Science Foundation CTS-0095098. The authors gratefully acknowledge helpful mathematical discussions with Professor Carl. M. Bender. Insightful comments and suggestions from Madan Somasi are also acknowledged.

Appendix A. Analytical expression for tube survival probability

For the fixed kinematics flow problems considered in this work, the material derivative in Eq. (3.14) can be equivalently replaced by the partial derivative,

$$\frac{\partial K}{\partial t} = \frac{1}{\pi^2\tau_d}\frac{\partial^2 K}{\partial s^2} - \frac{\partial}{\partial s}(\dot{s}_{tot}K) - \frac{\dot{\lambda}_{dissip}}{\lambda}K \tag{A.1}$$

As a first step towards the solution of Eq. (A.1) with the Eqs. (3.15) and (3.16), we introduce the following convenient change of variables to reduce the PDE, along with its initial condition and boundary conditions, to a standard form

$$L = \frac{1}{2}\sqrt{\frac{\pm\dot{\lambda}_{dissip}}{\lambda}\pi^2\tau_d}, \qquad x = (2s-1)L, \qquad y = \left[\frac{\pm\dot{\lambda}_{dissip}}{\lambda}\right](t-t') \tag{A.2}$$

$$\frac{\partial K}{\partial y} = \frac{\partial^2 K}{\partial x^2} \pm x\frac{\partial K}{\partial x} \tag{A.3}$$

where, $K = K(y, x) \in [0, 1]$, $x \in [-L, L]$, and $y \geq 0$. The negative sign is used in scaling when $\lambda \geq 1$ and the positive sign when $\lambda < 1$. Also the initial condition and the boundary conditions are now given by

$$K(y, x) = 1, \quad y = 0 \tag{A.4}$$

$$K(y, -L) = K(y, L) = 0, \quad y > 0 \tag{A.5}$$

The resulting PDE, Eq. (A.3), is now solved using the method of eigen function expansions. Solution to $K(y, x)$ is assumed to be separable and of the following form:

$$K(y,x) = \sum_{n=1}^{\infty} A_n(y) \cos\left[\frac{(2n-1)\pi x}{2L}\right] \tag{A.6}$$

Using the above expression in the PDE results in

$$\sum_{n=1}^{\infty} A_n'(y) \cos\left[\frac{(2n-1)\pi x}{2L}\right] = \sum_{n=1}^{\infty}\left[-\frac{(2n-1)^2\pi^2}{4L^2}\right] A_n(y) \cos\left[\frac{(2n-1)\pi x}{2L}\right] \pm \sum_{k=1}^{\infty}\left[-\frac{(2k-1)\pi x}{2L}\right] A_k(y) \sin\left[\frac{(2k-1)\pi x}{2L}\right] \tag{A.7}$$

We use another eigen function expansion to express $[-((2k-1)\pi x/2L)]\sin[((2k-1)\pi x/2L)]$, in terms of the cosines

$$\left[-\frac{(2k-1)\pi x}{2L}\right] \sin\left[\frac{(2k-1)\pi x}{2L}\right] = \sum_{n=1}^{\infty} C_{n,k} \cos\left[\frac{(2n-1)\pi x}{2L}\right], \quad k = 1, 2, 3, \ldots, \infty \tag{A.8}$$

Finally, using the above expression, Eq. (A.8), in Eq. (A.7) and comparing term by term, we get

$$A_n'(y) = -\left[\frac{(2n-1)^2\pi^2}{4L^2}\right] A_n(y) \pm \sum_{k=1}^{\infty} C_{n,k} A_k(y), \quad n = 1, 2, 3, \ldots, \infty \tag{A.9}$$

The coefficients $C_{n,k}$ are found by utilizing the orthogonality property of cosines. Therefore,

$$C_{n,k} = -\frac{1}{L}\int_{-L}^{L}\left[\left(\frac{(2k-1)\pi x}{2L}\right) \sin\left(\frac{(2k-1)\pi x}{2L}\right) \cos\left(\frac{(2n-1)\pi x}{2L}\right)\right] \mathrm{d}x, \quad n, k = 1, 2, 3, \ldots, \infty \tag{A.10}$$

Hence,

$$C_{n,k} = -\tfrac{1}{2}, \quad \text{if } n = k$$
$$C_{n,k} = \frac{(-1)^{k+n}(2k-1)(2n-1)}{2(k-n)(k+n-1)}, \quad \text{if } n \neq k \tag{A.11}$$

The functions $A_n(y)$ form a closed set of linear autonomous system of equations given by Eq. (A.9), which can be solved very easily using conventional methods. Due to the exponential nature of solution, the first few terms of this eigen function expansion, Eq. (A.6), are typically sufficient for reasonable accuracy and hence for all of our simulations the number of terms were restricted to 20. The initial condition required to solve the system of Equations, Eq. (A.9), is obtained from Eq. (A.4) and (A.6), again by utilizing the orthogonality property of cosines:

$$A_{n,0} = A_n(y=0) = \frac{1}{L}\int_{-L}^{L} \cos\left[\frac{(2n-1)\pi x}{2L}\right] \mathrm{d}x = \frac{4(-1)^{n+1}}{(2n-1)\pi} \tag{A.12}$$

It should be noted that use of the above technique of eigen function expansions, in solving for the tube survival probability, is also applicable for flows other than the fixed kinematics flows. However, the coefficients functions, A_n, in that case would need to be solved in an Eulerian finite element sense.

References

[1] P.G. de Gennes, Reptation of a polymer chain in the presence of fixed obstacles, J. Chem. Phys. 55 (1971) 572–579.
[2] M. Doi, S.F. Edwards, Dynamics of concentrated polymer systems. Part 1. Brownian motion in the equilibrium state, J. Chem. Soc. Faraday Trans. 2 74 (1978) 1789–1801.
[3] M. Doi, S.F. Edwards, Dynamics of concentrated polymer systems. Part 2. Molecular motion under flow, J. Chem. Soc. Faraday Trans. 2 74 (1978) 1802–1817.
[4] M. Doi, S.F. Edwards, Dynamics of concentrated polymer systems. Part 3. The constitutive equation, J. Chem. Soc. Faraday Trans. 2 74 (1978) 1818–1832.
[5] M. Doi, S.F. Edwards, Dynamics of concentrated polymer systems. Part 4. Rheological properties Brownian motion in the equilibrium state, J. Chem. Soc. Faraday Trans. 2 75 (1979) 38–54.
[6] C.C. Hua, J.D. Schieber, Segment connectivity, chain-length breathing, segmental stretch and constraint release in reptation models. I. Theory and single-step strain predictions, J. Chem. Phys. 109 (1998) 10018–10027.
[7] J. Fang, M. Kröger, H.C. Öttinger, A thermodynamically admissible reptation model for fast flow of entangled polymers. II. Model predictions for shear and extensional flows, J. Rheol. 44 (2000) 1293–1317.
[8] C. Tsenoglou, Viscoelasticity of binary homopolymer blends, ACS Polym. Preprints 28 (1987) 185–186.
[9] J. des Cloizeaux, Double reptation vs. simple reptation in polymer melts, Europhys. Lett. 5 (1988) 437–442.
[10] G. Marrucci, Dynamics of entanglements: a nonlinear model consistent with the Cox–Merz rule, J. Non-Newtonian Fluid Mech. 62 (1996) 279–289.
[11] G. Ianniruberto, G. Marrucci, On the compatibility of the Cox–Merz rule with the model of Doi and Edwards, J. Non-Newtonian Fluid Mech. 65 (1996) 241–246.
[12] G. Marrucci, N. Grizzuti, Fast flow of entangled polymers: predictions of the tube model on chain stretching, Gazz. Chim. Ital. 118 (1988) 179–185.
[13] G. Marrucci, F. Greco, G. Ianniruberto, Integral and differential constitutive equations for entangled polymers with simple versions of CCR and force balance on entanglements, Rheo. Acta 40 (2000) 98–103.
[14] H.C. Öttinger, A thermodynamically admissible reptation model for fast flow of entangled polymers, J. Rheo. 43 (1999) 1461–1493.
[15] D.W. Mead, R.G. Larson, M. Doi, A molecular theory for fast flow of entangled polymers, Macromolecules 31 (1998) 7895–7914.
[16] C.C. Hua, J.D. Schieber, D.C. Venerus, Segment connectivity, chain-length breathing, segmental stretch and constraint release in reptation models. II. Double-step strain predictions, J. Chem. Phys. 109 (1998) 10028–10032.
[17] C.C. Hua, J.D. Schieber, D.C. Venerus, Segment connectivity, chain-length breathing, segmental stretch and constraint release in reptation models. III. Shear flows, J. Rheol. 43 (1999) 701–717.
[18] A.P.G. van Heel, M.A. Hulsen, B.H.A.A. van den Brule, Simulation of the Doi–Edwards model in complex flow, J. Rheo. 43 (1999) 1239–1260.
[19] E.A.J.F. Peters, A.P.G. van Heel, M.A. Hulsen, B.H.A.A. van den Brule, Generalization of the deformation field method to simulate advanced reptation models in complex flow, J. Rheol. 44 (2000) 811–829.
[20] M.A. Hulsen, A.P.G. van Heel, B.H.A.A. van den Brule, Simulation of viscoelastic flows using Brownian configuration fields, J. Non-Newtonian Fluid Mech. 70 (1997) 79–101.
[21] E.A.J.F. Peters, M.A. Hulsen, B.H.A.A. van den Brule, Instationary Eulerian viscoelastic flow simulations using time separable Rivlin–Sawyers constitutive equations, J. Non-Newtonian Fluid Mech. 89 (2000) 209–228.
[22] P. Wapperom, R. Keunings, Simulation of linear polymer melts in transient complex flow, J. Non-Newtonian Fluid Mech. 95 (2000) 67–83.
[23] M. Laso, H.C. Öttinger, Calculation of viscoelastic flow using molecular models: the CONNFFESSIT approach, J. Non-Newtonian Fluid Mech. 47 (1993) 1–20.
[24] H.C. Öttinger, B.H.A.A. van den Brule, M.A. Hulsen, Brownian configuration fields and variance reduced CONNFFESSIT, J. Non-Newtonian Fluid Mech. 70 (1997) 255–261.

[25] P. Halin, R. Keunings, V. Legat, The Lagrangian particle method for macroscopic and micro-macro viscoelastic flow computations, J. Non-Newtonian Fluid Mech. 79 (1998) 387–403.
[26] X. Gallez, P. Halin, G. Lielens, R. Keunings, V. Legat, The adaptive Lagrangian particle method for microscopic and micro-macro computations of time-dependent viscoelastic flows, Comp. Meth. Appl. Mech. Eng. 180 (1999) 345–364.
[27] P. Wapperom, R. Keunings, V. Legat, The backward-tracking Lagrangian particle method for transient viscoelastic flows, J. Non-Newtonian Fluid Mech. 91 (2000) 273–295.
[28] R.B. Bird, C.F. Curtiss, R.C. Armstrong, O. Hassager, Dynamics of polymeric liquids, Kinetic Theory, 2nd ed., vol. 2, Wiley-Interscience, New York, 1987.
[29] H.C. Öttinger, Stochastic Processes in Polymeric Fluids, Springer, Berlin, 1996.
[30] W.P. Petersen, Lagged fibonacci random number generators for the NEC SX-3, Int. J. High Speed Comp. 37 (1994) 106–119.